

Published in final edited form as:

*J Immunol.* 2016 April 15; 196(8): 3452–3459. doi:10.4049/jimmunol.1502601.

## TRIM21 Immune Signaling Is More Sensitive to Antibody Affinity Than Its Neutralization Activity

Stian Foss<sup>#,\*†</sup>, Ruth E. Watkinson<sup>#‡</sup>, Algirdas Grevys<sup>\*,†</sup>, Martin B. McAdam<sup>†</sup>, Malin Bern<sup>\*,†</sup>, Lene Stokken Høydahl<sup>\*,†</sup>, Bjørn Dalhus<sup>§</sup>, Terje E. Michaelsen<sup>¶,||</sup>, Inger Sandlie<sup>\*,†</sup>, Leo C. James<sup>‡</sup>, and Jan Terje Andersen<sup>\*,†</sup>

<sup>\*</sup>Centre for Immune Regulation, Department of Biosciences, University of Oslo, N-0371 Oslo, Norway

<sup>†</sup>Centre for Immune Regulation, Department of Immunology, Oslo University Hospital Rikshospitalet, University of Oslo, N-0424 Oslo, Norway

<sup>‡</sup>Protein and Nucleic Acid Chemistry Division, Medical Research Council Laboratory of Molecular Biology, Cambridge CB2-0QH, United Kingdom

<sup>§</sup>Department of Microbiology, Oslo University Hospital Rikshospitalet, University of Oslo, Oslo N-0424, Norway

<sup>¶</sup>Department of Bacteriology and Immunology, Norwegian Institute of Public Health, N-0403 Oslo, Norway

<sup>||</sup>Department of Chemical Pharmacy, School of Pharmacy, University of Oslo, N-0316 Oslo, Norway

<sup>#</sup> These authors contributed equally to this work.

### Abstract

Ab-coated viruses can be detected in the cytosol by the FcR tripartite motif-containing 21 (TRIM21), which rapidly recruits the proteasomal machinery and triggers induction of immune signaling. As such, TRIM21 plays a key role in intracellular protection by targeting invading viruses for destruction and alerting the immune system. A hallmark of immunity is elicitation of a balanced response that is proportionate to the threat, to avoid unnecessary inflammation. In this article, we show how Ab affinity modulates TRIM21 immune function. We constructed a humanized monoclonal IgG1 against human adenovirus type 5 (AdV5) and a panel of Fc-engineered variants with a wide range of affinities for TRIM21. We found that IgG1-coated viral particles were neutralized via TRIM21, even when affinity was reduced by as much as 100-fold. In contrast, induction of NF- $\kappa$ B signaling was more sensitive to reduced affinity between TRIM21 and the Ab variants. Thus, TRIM21 mediates neutralization under suboptimal conditions, whereas

---

Address correspondence and reprint requests to Prof. Jan Terje Andersen, Center for Immune Regulation and Department of Immunology, Oslo University Hospital and University of Oslo, P.O. Box 4956, N-0424 Oslo, Norway. j.t.andersen@medisin.uio.no. S.F., R.E.W., I.S., L.C.J., and J.T.A. designed research. S.F., R.E.W., A.G., and M.B.M. performed experiments. B.D., M.B., T.E.M., and L.S.H. contributed reagents/ analytical tools. S.F., I.S., L.C.J., and R.E.W. analyzed data. S.F., L.C.J., and J.T.A. wrote the manuscript.

### Disclosures

The authors have no financial conflicts of interest.

induction of immune signaling is balanced according to the functional affinity for the incoming immune stimuli. Our findings have implications for engineering of antiviral IgG therapeutics with tailored effector functions.

Once Abs are bound to their target pathogen, they induce a broad range of effector mechanisms via their Fc by interacting with classical Fc $\gamma$ Rs expressed on the surface of immune cells (1, 2). However, Abs are also carried inside the cytosol of cells during viral infection (3). In the cytosol, tripartite motif-containing 21 (TRIM21) binds the Fc of virus-associated Abs and targets the complex for proteasomal degradation in a process termed Ab-dependent intracellular neutralization (ADIN). ADIN is a remarkably efficient process, requiring as few as two Ab molecules/virus for elimination to occur (4). In addition, TRIM21 stimulates inflammatory signaling and activates innate transcription factors, such as NF- $\kappa$ B (5). Both the effector and sensory responses are dependent on TRIM21 autoubiquitination that is mediated by the sequential action of the E2 ubiquitin-conjugating enzymes Ube2W and Ube2N/Ube2V (3, 5, 6). Specifically, upon recognition of viral-IgG complexes, TRIM21 is monoubiquitinated by Ube2W and then polyubiquitinated via a K63 linkage by Ube2N/Ube2V2. TRIM21 is subsequently modified with K48-linked ubiquitin chains. Upon proteasomal recruitment, the anchored K63-linked ubiquitin chains are cleaved from TRIM21 by the action of the proteasomal deubiquitinase Poh1, stimulating innate immune signaling (7). This complex mechanism ensures synchronized activation of the dual effector and sensor functions of TRIM21. In addition, TRIM21-mediated ADIN results in release of the viral genome that can be detected by the cytosolic RNA sensor RIG-1 or the cytosolic DNA sensor cGAS (8). This results in two distinct waves of TRIM21-dependent immune signaling.

TRIM21 is ubiquitously expressed by hematopoietic and nonhematopoietic cells (9) and is a multidomain protein consisting of an N-terminal RING domain with E3 ubiquitin ligase activity, a B-box domain, a coiled-coil domain, and a C-terminal PRYSPRY domain that harbors the Ab binding site (10). The binding site on IgG is located in the C<sub>H</sub>2-C<sub>H</sub>3 elbow region of the Fc, and overlaps with the binding site for the neonatal FcR (FcRn) (11, 12), as well as several pathogen-derived FcRs (13–15). The affinity of a single PRYSPRY domain for IgG is ~200 nM (10), and the interaction is conserved in mammals (16). However, TRIM21 is dimeric, allowing simultaneous binding to both H chains, which greatly enhances the interaction strength. Dimeric TRIM21 binds IgG strongly, with an affinity of 0.6 nM, and is the highest-affinity Fc receptor in mammals (3). As a result of this mode of binding, TRIM21 has remarkably broad Ab isotype specificity because it also binds IgA and IgM, although with lower affinity (3, 17). The importance of TRIM21 in systemic Ab-dependent viral protection was demonstrated in a mouse adenovirus type 1 infection model (18).

Although TRIM21 mediates synchronized effector and immune signaling responses, it is not known whether these two outputs are differentially regulated. In this study, we investigated how the magnitude of TRIM21 responses is influenced by the strength of interaction with incoming Ab-virus complexes. To this end, we constructed a humanized monoclonal IgG1 Ab with specificity for human adenovirus type 5 (AdV5) and designed a panel of Fc-

engineered variants with a range of distinct binding affinities toward TRIM21. We found that TRIM21-mediated ADIN occurred even when binding affinity was reduced by up to 100-fold, whereas induction of NF- $\kappa$ B signaling was highly sensitive to affinity reductions. Thus, ADIN remains effective under suboptimal conditions, but NF- $\kappa$ B signaling is only induced above a threshold of immune complex detection. Our findings have implications for the development of Fc-engineered antiviral IgG therapeutics with optimal effector functions.

## Materials and Methods

### Cell culture

The cell lines HEK293E, HEK293T, and HeLa were maintained in DMEM supplemented with 10% FBS, 100 U/ml penicillin, and 100  $\mu$ g/ml streptomycin at 37°C in a humid 5% CO<sub>2</sub>, 95% air incubator. Where appropriate, cells were selected in 1 mg/ml G418 (Life Technologies). Mouse embryonic fibroblasts (MEFs) were derived from wild-type (WT) C57BL/6 or TRIM21-knockout (K21) embryos, as described (4).

### Virus production

Replication-deficient AdV5 carrying the GFP reporter gene (AdV5-GFP) was grown in *trans*-complementation cell line 293F for 72 h before three rounds of freeze-thaw, to release virus particles, and filtration at 0.45  $\mu$ m. Virus stocks were purified by two rounds of ultracentrifugation banding on a cesium chloride gradient, dialyzed into PBS/10% glycerol, and frozen at -80°C until required.

### Production of recombinant TRIM21

Recombinant TRIM21 PRYSPRY was overexpressed in BL21 *Escherichia coli* cells under standard conditions and purified by Ni-NTA resin (QIAGEN) and Superdex 75 gel filtration (GE Healthcare), as described (10). Full-length maltose-binding protein (MBP)-tagged human TRIM21 was expressed in *E. coli* and purified using amylose resin and size-exclusion chromatography, as described (10).

### Construction and production of humanized 9C12

Vectors encoding humanized 9C12 (h9C12) variants were based on the pLNOH2/pLNOK expression system (19). Specifically, H and L chain V genes derived from the hybridoma cell line TC31-9C12.C9 (Developmental Studies Hybridoma Bank, University of Iowa, Iowa City, Iowa) were synthesized as a cloning cassette flanked by the restriction sites recognized by the endonucleases BsmI/BsiWI. The gene fragments were then subcloned into pLNOH2-N<sup>IP</sup>hIgG1-WT-oriP and N<sup>IP</sup>pLNOK-oriP, resulting in pLNOH2-Hexon<sup>h</sup>hIgG1-WT-oriP and Hexon<sup>p</sup>pLNOK-oriP encoding a chimeric human H chain and L chain, respectively. The H chain vector pLNOH2-Hexon<sup>h</sup>hIgG1-WT-oriP was further used for the generation of h9C12 variants by exchanging C<sub>H</sub>2 and C<sub>H</sub>3 gene fragments with fragments containing the desired mutations. C<sub>H</sub>2 fragments were exchanged using the unique restriction sites recognized by the endonucleases AgeI and SfiI, whereas C<sub>H</sub>3 fragments were exchanged using SfiI and BamHI (All from New England Biolabs). Following cotransfection of both H chain and L chain vectors into HEK293E cells using Lipofectamine 2000 (Life

Technologies), h9C12 variants were purified from collected supernatant using a C<sub>H</sub>1-specific CaptureSelect column (Life Technologies).

Monomeric fractions were isolated by size-exclusion chromatography using a Superdex 200 column (GE Healthcare). Protein integrity was verified by nonreducing SDS-PAGE (Life Technologies).

### Immunoblotting

Cells from a single well of a 24-well plate were scraped off, resuspended, and heated at 98°C for 5 min in 100 µl 1× LDS sample buffer with reducing agent (Life Technologies). Equal volumes were loaded onto a 4–12% NuPAGE gel and electrophoresed in 1× MOPS buffer (Life Technologies). Proteins were transferred onto a Protran nitrocellulose membrane (Whatman) and immunoblotted with either a mouse monoclonal anti-TRIM21 Ab (Santa Cruz Biotechnology) or rabbit polyclonal anti-β-actin Ab (Cell Signaling). In all cases, blots were incubated with Ab in PBS containing 5% milk and 0.1% Tween and washed with PBS-Tween. Visualization was carried out using an ECL Plus Western Blotting Detection System (GE Healthcare).

### Protein stability by differential scanning fluorimetry

Protein stability of monomeric IgG1 variants was measured by differential scanning fluorimetry (DSF) using a LightCycler RT-PCR instrument (Roche). SYPO Orange (Sigma-Aldrich) was used at a 1:1000 dilution, and the protein concentration was 0.1 mg/ml in a final volume of 25 µl. All samples were run in triplicates in a 96-well LightCycler 480 Multiwell Plate. The peaks of excitation and emission of SYPO Orange are 490 and 580 nm, respectively. The 450-nm excitation and 568-nm emission filters on the RT-PCR instrument were used. The RT-PCR instrument was programmed to raise the temperature from 25 to 95°C after a stabilization period of 10 min at 25°C. Two measurements at each temperature were recorded, and data were collected every 0.5°C. Data transformation and analysis were performed using the DSF analysis protocol (20).

### ELISA

Recombinant AdV5 hexon (AbD Serotec) (diluted to 1 µg/ml in PBS), a polyclonal anti-human Fc Ab produced in goat (locally produced; diluted to 1 µg/ml in PBS), or AdV5-GFP (Sino Biologicals) (diluted 1:1000 in PBS from a  $1.0 \times 10^{10}$  PFU/ml viral stock) was coated in 96-well plates (Nunc) and incubated overnight at 4°C. Remaining surface area was blocked using PBS/4% skim milk (S) (Acumedia), before washing four times with PBS/0.005% Tween 20 (T). Titrated amounts of h9C12 variants diluted in PBS/T/S were added to the wells and incubated for 1 h at room temperature (RT). Following washing as above, MBP-tagged full-length human TRIM21 or an alkaline phosphatase (ALP)-conjugated polyclonal anti-human Fc Ab from goat (Sigma-Aldrich), each diluted to 1 µg/ml in PBS/S/T, was added and incubated for 1 h at RT. Following washing as above, bound MBP-tagged full-length human TRIM21 was detected by an HRP-conjugated anti-MBP Ab (New England Biolabs). Binding was visualized by addition of tetramethylbenzidine solution (Calbiochem) or ALP substrate (Sigma-Aldrich). The HRP-tetramethylbenzidine reaction

was terminated by addition of 100  $\mu$ l 1 M HCl, and the 450-nm (HRP) or 405-nm (ALP) absorption spectrum was recorded using a Sunrise plate reader (TECAN).

### Surface plasmon resonance

A Biacore 3000 instrument (GE Healthcare) was used for all kinetics measurements. h9C12 variants were immobilized by amine coupling on CM5 sensor chips, according to the manufacturer's instructions. The coupling was performed by injecting 1–2.5  $\mu$ g/ml the IgG1 variants dissolved in 10 mM sodium acetate (pH 4.5) (GE Healthcare). HBS-P buffer (0.01 M HEPES, 0.15 NaCl, 0.005% surfactant P20 [pH 7.4]) was used as running and dilution buffer. Subsequently, concentration series of recombinant human TRIM21 PRYSPRY were injected. Kinetics analysis was performed using BIAevaluation software, and the binding data were fitted to a simple first-order (1:1) Langmuir biomolecular interaction model. Steady-state  $K_D$  values were obtained by immobilizing h9C12 variants at ~2500 RU and determined by an equilibrium (Req) binding model.

### Neutralization assay

HeLa cells were plated at a density of  $6 \times 10^4$  cells/well in 24-well plates 1 d prior to infection. A total of  $2.5 \times 10^4$  infectious units of AdV5-GFP was mixed 1:1 with Ab, to give the final stated Ab concentration, and incubated for 30 min at RT. This was added to the cells and allowed to incubate for 24 h at 37°C. Cells were then collected by trypsinization and fixed in 4% paraformaldehyde solution. AdV5-GFP reporter gene expression was determined by FACS analysis. Where stated, cells were transfected with 150 pmol control or TRIM21 small interfering RNA (siRNA), following the manufacturer's instructions (Life Technologies). Relative infection was calculated as described (4).

### NF- $\kappa$ B reporter assay

HEK293T cells stably transfected with pGL4.32 NF- $\kappa$ B luciferase (Promega) were plated at a density of  $1 \times 10^4$  cells/well in 96-well plates 1 d prior to infection. AdV5-GFP was mixed 1:1 with Ab, to give the final Ab concentration, and incubated for 30 min at RT. AdV5-GFP was used at a final concentration of  $7.4 \times 10^5$  infectious units/well. This was added to cells and allowed to incubate for 7 h at 37°C before the addition of 100  $\mu$ l steadylite plus luciferase reagent (Perkin Elmer) and analysis using a BMG PHERAstar FS plate reader. Where stated, cells were transfected with 150 pmol control or TRIM21 siRNA following the manufacturer's instructions (Life Technologies).

### Statistical analysis

Figures were generated and statistical analyses were performed using GraphPad Prism version 6.0 (GraphPad). All h9C12 variants were tested at least three times, and error bars represent SD from one representative experiment. The multiple unpaired *t* test or one-way ANOVA test (Dunnett) was used to calculate the statistical significance. A *p* value < 0.05 was considered significant.

## Results

### Construction of a mouse–human chimeric anti-AdV5 mAb

Studies on TRIM21 function have been performed using a range of polyclonal sera from different species but only monoclonal Abs from mice (4). To characterize the Ab determinants of TRIM21 function in more detail, we first generated a humanized mAb directed toward human AdV5, h9C12, consisting of the H chain of human IgG1 and a human  $\kappa$  L chain paired with the variable genes derived from the hybridoma 9C12, a nonneutralizing Ab specific for the major capsid protein, hexon (21). Pure monomeric h9C12 was obtained from transiently transfected adherent HEK293E cells, followed by purification on a CaptureSelect affinity matrix specific for the C<sub>H</sub>1 domain and size-exclusion chromatography (Fig. 1A). The h9C12 Ab bound strongly to its cognate hexon Ag in ELISA (Fig. 1B). To assess the impact of humanization on TRIM21 activity, HeLa cells were pretreated with TRIM21 siRNA or control siRNA (Fig. 1C), and h9C12 incubated with replication-deficient human AdV5-GFP (22) was allowed to infect the cells. h9C12 efficiently neutralized AdV5-GFP, and this activity was considerably reduced in cells treated with TRIM21 siRNA (Fig. 1D). In contrast to the hybridoma-derived mouse 9C12 (Fig. 1E), h9C12 showed 9-fold retained neutralization activity at the highest concentration when cells were treated with TRIM21 siRNA. The reason for this is unknown, but it might be explained by incomplete TRIM21 knockdown. h9C12 could also be used by mouse TRIM21 to prevent infection, as shown by a comparison of the difference in ADIN activity induced by 9C12 and h9C12 in WT (TRIM21<sup>+/+</sup>) and K21 (TRIM21<sup>-/-</sup>) MEFs (Fig. 1F). We showed previously that TRIM21 targets 9C12-bound AdV5 for proteasomal degradation (3). To address whether h9C12-dependent ADIN occurred following the same mechanism, HeLa cells were treated with the proteasome inhibitor epoxomicin or DMSO prior to AdV5-GFP infection with the parental 9C12 or h9C12. The results showed that inhibition of the proteasome abrogated the cytosolic neutralization activity of both Abs (Fig. 1G).

Next, we tested the capacity of h9C12 to induce TRIM21-dependent NF- $\kappa$ B activation. AdV5-GFP, alone or in complex with h9C12, was added to HEK293T cells stably transfected with an NF- $\kappa$ B luciferase reporter vector pretreated with TRIM21 siRNA or control siRNA. AdV5-GFP alone did not stimulate signaling, whereas the complex with h9C12 induced a dose-dependent increase in NF- $\kappa$ B activity (Fig. 1H). Together, these experiments show that h9C12 is recognized by TRIM21 and promotes ADIN activity and NF- $\kappa$ B signaling.

### Fc engineering of h9C12 variants

We used the previously solved cocrystal structure of the human PRYSPRY domain in complex with an IgG1 Fc fragment (10) to design a range of h9C12 variants with different affinities for TRIM21 (Fig. 2A). The PRYSPRY domain binds to both H chains of the homodimeric Fc at the interface between the C<sub>H</sub>2 and C<sub>H</sub>3 domains, where I253, H433, N434, and H435 are directly engaged in binding. A panel of mutant h9C12 variants was made by targeting these positions by site-directed mutagenesis, and variants were produced in HEK293E cells (Fig. 2B). As a control, H310 was mutated because it is not directly involved in the interaction. The amounts of h9C12 variants used in all binding and cellular

assays were controlled by an anti-human Fc ELISA (Supplemental Fig. 1), and DSF analysis showed that none of the introduced mutations destabilized IgG (Fig. 2C). Further, the importance of the individual interactions was determined by measuring binding to full-length human TRIM21 by ELISA (Fig. 2D) and the derived monomeric PRYSPRY domain by surface plasmon resonance (SPR) (Fig. 3, Table I, Supplemental Fig. 2). Both assays showed a similar hierarchy of binding as follows: WT = H310A > I253A > N434A > N434S > N434D > H433K > H433A. Although H310A did not have any impact on binding, the other Ab mutants bound with  $K_D$  values ranging from 2-fold reduced binding (I253A) to a >100-fold reduction (H433K). Only a negligible binding response was measured for H433A. The importance of the Fc residues 433–435 in TRIM21 binding correlates with their proximity to the hot-spot residues D355, W381, W383, and D452 within the TRIM21 PRYSPRY domain (10). Moreover, h9C12 with the C<sub>H</sub>2 substitutions L235A and P329A (Fig. 4A), which eliminate binding to Fc $\gamma$ Rs and C1q (23, 24), respectively, did not affect TRIM21 binding, ADIN, or NF- $\kappa$ B induction (Fig. 4B–E). Thus, the binding sites for Fc $\gamma$ Rs/C1q can be manipulated without affecting TRIM21 activity. Importantly, the engineered h9C12 variants bound equally well to recombinant AdV5 hexon and AdV5-GFP virus particles in ELISA (Supplemental Fig. 1).

### TRIM21-induced NF- $\kappa$ B induction is more sensitive to IgG affinity than ADIN

To explore how affinity affects ADIN activity and induction of NF- $\kappa$ B, a titration series of Ab variants was preincubated with AdV5-GFP and added to HeLa cells or HEK293T NF- $\kappa$ B luciferase reporter cells. The results showed that induction of NF- $\kappa$ B signaling was affected more severely by affinity reductions compared with ADIN activity. In addition, the relative effect of affinity on activity was noticeably influenced by Ab opsonization (Fig. 5). To investigate this in more detail, we compared the level of ADIN activity and NF- $\kappa$ B induction at low, intermediate, and high levels of Ab opsonization. This revealed that, at low Ab concentration, ADIN is relatively insensitive to reductions in affinity toward the incoming immune complex. Specifically, I253A, which has a 2-fold reduced affinity for TRIM21, showed equal ADIN activity as WT, whereas the variants with 10–20-fold reduced affinity for TRIM21 still conferred moderate activity (Fig. 5A). Measurable ADIN activity could even be observed for H433K, which has a 100-fold reduced affinity for TRIM21. Importantly, H433A, which does not bind TRIM21, completely abolished ADIN and phenocopied the activity of WT h9C12 in TRIM21-depleted cells (Supplemental Fig. 3).

At low levels of Ab opsonization, induction of NF- $\kappa$ B by TRIM21 was significantly more sensitive to Ab affinity than ADIN, because all Fc-engineered variants, with the exception of H310A, resulted in reduced NF- $\kappa$ B induction (Fig. 5B). This was particularly clear for I253A, which resulted in a >10-fold lower response compared with WT. To directly compare the effect of Ab affinity on ADIN and NF- $\kappa$ B induction, we plotted the relative activities of each variant with respect to WT against the measured  $K_D$  (Fig. 5C). This revealed that, at low Ab opsonization, induction of NF- $\kappa$ B signaling is clearly more sensitive to alterations in IgG affinity than ADIN. This was also the case at intermediate levels of Ab opsonization (Fig. 5D–F). However, the reduction in NF- $\kappa$ B signaling as a result of reduced affinity is less dramatic and more proportional to ADIN at high levels of Ab opsonization (Fig. 5G–I). This

suggests the presence of a threshold level below which signaling is not triggered. In contrast, ADIN is achieved even at low levels of Ab variants with reduced affinity.

## Discussion

TRIM21 has effector and signaling functions in nonhematopoietic cells, but each has different regulatory requirements. To be fully protective, effector function in the form of neutralization must be capable of reducing infection when TRIM21 recruitment to Ab–viral complexes is suboptimal. In contrast, because NF- $\kappa$ B activation can lead to systemic inflammatory changes in the host, it must be tightly controlled to prevent spurious activation (25, 26). In this study, we show that modulating the binding affinity of the TRIM21–IgG interaction has a less dramatic impact on ADIN than on the induction of NF- $\kappa$ B signaling. Recently, TRIM21 was shown to induce an initial Ab-driven direct innate immune response that was followed by a delayed response upon TRIM21-induced exposure of the viral genome (8). Although we did not separate these events in this study, our data suggest that the dual effector and sensory functions of TRIM21 differ in their responsiveness depending on the functional affinity for the incoming Abs. Setting a threshold for activation is a common strategy in immune signaling; TCR activation requires a minimum receptor residency, whereas Fc $\gamma$ R activation is governed, in part, by the integration of signals from activating Fc $\gamma$ Rs and the inhibitory Fc $\gamma$ RIIb (1).

We humanized a nonentry blocking anti-AdV5 Ab, h9C12, which was found to mediate ADIN and induce NF- $\kappa$ B in a TRIM21-dependent manner. By engineering the Fc part of h9C12, we generated AdV5–IgG immune complexes with different binding affinities (2- to >100-fold reduction) to TRIM21. Importantly, none of the mutations introduced in the constant Fc part of h9C12 affected the ability to interact with its cognate Ag. Receptor-binding kinetics were determined by SPR analysis, where a monomeric version of the IgG-binding TRIM21 PRYSPRY domain was injected over immobilized h9C12 Abs, and  $K_D$  values were derived by fitting the sensorgrams to a simple 1:1 interaction model or steady-state affinity model. We also measured relative binding of the h9C12 variants to full-length TRIM21 by ELISA, which gave rise to the same hierarchy of binding as that determined by SPR. Notably, we found that ADIN activity was affected, but not completely abolished, even though monomeric affinity was reduced by >100-fold (H433K). To completely abolish ADIN activity, binding had to be almost completely eliminated, as shown for the H433A mutant. In stark contrast, a reduction in affinity of only 2-fold (I253A) resulted in severely impaired NF- $\kappa$ B induction. We found that the difference between NF- $\kappa$ B induction and ADIN was most prominent at low levels of opsonization, whereas at high levels of opsonization, NF- $\kappa$ B induction correlated more closely with ADIN activity, suggesting the presence of different activation thresholds. Although the mechanism responsible for this difference is unclear, it is likely regulated by the complex ubiquitination and deubiquitination activities acting downstream of TRIM21 (3, 5, 6). In addition, elimination of adenovirus via ADIN correlated with disposal of bound IgG (3), suggesting that the signaling response is also potentially self-limiting. Therapeutically, mAbs are increasingly being considered as attractive agents to fight viral infections. Thus, our data may be of importance for the development of such Abs, for which tuning of Fc-mediated effector functions is receiving increasing interest (27). For instance, IgG variants with a modest

reduction in affinity toward TRIM21 might be used to avoid induction of strong immune signaling via NF- $\kappa$ B activation, without compromising efficient neutralization. Also, because IgG binding to Fc $\gamma$ Rs and C1q can be manipulated independently of TRIM21 functions, distinct Fc effector functions may be tailored for a particular antiviral IgG of interest.

From a biological perspective, our data are interesting in light of previous reports demonstrating that TRIM21 binds IgG, as well as IgA and IgM (3, 17). Using fluorescence anisotropy, IgM and IgA were found to bind the PRYSPRY domain with a monomeric affinity of 17 and 50  $\mu$ M, respectively; however, dimeric binding to full-length TRIM21 is postulated to result in sub-micromolar affinity at physiological conditions (17). Structurally, the remarkable broad Ab specificity of TRIM21 is thought to be due to amino acid differences in the Fc loop, which protrudes into the hydrophobic binding pocket on the PRYSPRY domain (17). Cellular studies demonstrated that IgM and IgA activate ADIN and induce NF- $\kappa$ B signaling (3, 5, 17). Although a side-by-side comparison of humanized versions of IgA, IgM, and IgG with the same epitope specificity is needed to fully address the impact of affinity on TRIM21 functions, our data hint that the lower affinity of IgA and IgM will likely have the greatest impact on immune signaling via TRIM21. However, because IgA and IgM form dimers and pentamers, respectively, their lower affinity for TRIM21 may be offset by their increased avidity for Ag. Thus, the impact of avidity and complex formation on ADIN and signaling should be addressed in future studies.

## Supplementary Material

Refer to Web version on PubMed Central for supplementary material.

## Acknowledgments

This work was supported in part by the Research Council of Norway through its Center of Excellence funding scheme (Project 179573). J.T.A. was supported by the Research Council of Norway (Grants 230526/F20 and 179573/V40). M.B.M. was supported by the Research Council of Norway (Grant 179573/V40). M.B. was supported by the Research Council of Norway through its program for Global Health and Vaccination Research (Grant 143822). S.F. and A.G. were supported by the University of Oslo. L.C.J. and R.E.W. were supported by the Medical Research Council (UK; U105181010) and the European Research Council (281627-IAI).

## Abbreviations used in this article:

<b>ADIN</b>	Ab-dependent intracellular neutralization
<b>AdV5</b>	adenovirus type 5
<b>AdV5-GFP</b>	AdV5 carrying the GFP reporter gene
<b>ALP</b>	alkaline phosphatase
<b>DSF</b>	differential scanning fluorimetry
<b>h9C12</b>	humanized 9C12
<b>K21</b>	TRIM21 knockout

<b>MBP</b>	mannose-binding protein
<b>MEF</b>	mouse embryonic fibroblast
<b>RT</b>	room temperature
<b>S</b>	4% skim milk
<b>siRNA</b>	small interfering RNA
<b>SPR</b>	surface plasmon resonance
<b>T</b>	0.05% Tween 20
<b>TRIM21</b>	tripartite motif-containing 21
<b>WT</b>	wild-type

## References

1. Nimmerjahn F, Ravetch JV. Fcγ receptors as regulators of immune responses. *Nat Rev Immunol.* 2008; 8:34–47. [PubMed: 18064051]
2. Hogarth PM, Pietersz GA. Fc receptor-targeted therapies for the treatment of inflammation, cancer and beyond. *Nat Rev Drug Discov.* 2012; 11:311–331. [PubMed: 22460124]
3. Mallery DL, McEwan WA, Bidgood SR, Towers GJ, Johnson CM, James LC. Antibodies mediate intracellular immunity through tripartite motif-containing 21 (TRIM21). *Proc Natl Acad Sci USA.* 2010; 107:19985–19990. [PubMed: 21045130]
4. McEwan WA, Hauler F, Williams CR, Bidgood SR, Mallery DL, Crowther RA, James LC. Regulation of virus neutralization and the persistent fraction by TRIM21. *J Virol.* 2012; 86:8482–8491. [PubMed: 22647693]
5. McEwan WA, Tam JC, Watkinson RE, Bidgood SR, Mallery DL, James LC. Intracellular antibody-bound pathogens stimulate immune signaling via the Fc receptor TRIM21. *Nat Immunol.* 2013; 14:327–336. [PubMed: 23455675]
6. Fletcher AJ, Mallery DL, Watkinson RE, Dickson CF, James LC. Sequential ubiquitination and deubiquitination enzymes synchronize the dual sensor and effector functions of TRIM21. *Proc Natl Acad Sci USA.* 2015; 112:10014–10019. [PubMed: 26150489]
7. Fletcher AJ, Mallery DL, Watkinson RE, Dickson CF, James LC. Sequential ubiquitination and deubiquitination enzymes synchronize the dual sensor and effector functions of TRIM21. *Proc Natl Acad Sci USA.* 2015; 112:10014–10019. [PubMed: 26150489]
8. Watkinson RE, McEwan WA, Tam JC, Vaysburd M, James LC. TRIM21 Promotes cGAS and RIG-I Sensing of Viral Genomes during Infection by Antibody-Opsonized Virus. *PLoS Pathog.* 2015; 11:e1005253. [PubMed: 26506431]
9. Reymond A, Meroni G, Fantozzi A, Merla G, Cairo S, Luzi L, Riganelli D, Zanaria E, Messali S, Cainarca S, et al. The tripartite motif family identifies cell compartments. *EMBO J.* 2001; 20:2140–2151. [PubMed: 11331580]
10. James LC, Keeble AH, Khan Z, Rhodes DA, Trowsdale J. Structural basis for PRYSPRY-mediated tripartite motif (TRIM) protein function. *Proc Natl Acad Sci USA.* 2007; 104:6200–6205. [PubMed: 17400754]
11. Burmeister WP, Huber AH, Bjorkman PJ. Crystal structure of the complex of rat neonatal Fc receptor with Fc. *Nature.* 1994; 372:379–383. [PubMed: 7969498]
12. Oganessian V, Damschroder MM, Cook KE, Li Q, Gao C, Wu H, Dall'Acqua WF. Structural insights into neonatal Fc receptor-based recycling mechanisms. *J Biol Chem.* 2014; 289:7812–7824. [PubMed: 24469444]

13. Deisenhofer J. Crystallographic refinement and atomic models of a human Fc fragment and its complex with fragment B of protein A from *Staphylococcus aureus* at 2.9- and 2.8-Å resolution. *Biochemistry*. 1981; 20:2361–2370. [PubMed: 7236608]
14. Kato K, Lian LY, Barsukov IL, Derrick JP, Kim H, Tanaka R, Yoshino A, Shiraiishi M, Shimada I, Arata Y, et al. Model for the complex between protein G and an antibody Fc fragment in solution. *Structure*. 1995; 3:79–85. [PubMed: 7743134]
15. Sprague ER, Wang C, Baker D, Bjorkman PJ. Crystal structure of the HSV-1 Fc receptor bound to Fc reveals a mechanism for antibody bipolar bridging. *PLoS Biol*. 2006; 4:e148. [PubMed: 16646632]
16. Keeble AH, Khan Z, Forster A, James LC. TRIM21 is an IgG receptor that is structurally, thermodynamically, and kinetically conserved. *Proc Natl Acad Sci USA*. 2008; 105:6045–6050. [PubMed: 18420815]
17. Bidgood SR, Tam JC, McEwan WA, Mallery DL, James LC. Translocalized IgA mediates neutralization and stimulates innate immunity inside infected cells. *Proc Natl Acad Sci USA*. 2014; 111:13463–13468. [PubMed: 25169018]
18. Vaysburd M, Watkinson RE, Cooper H, Reed M, O'Connell K, Smith J, Cruickshanks J, James LC. Intracellular antibody receptor TRIM21 prevents fatal viral infection. *Proc Natl Acad Sci USA*. 2013; 110:12397–12401. [PubMed: 23840060]
19. Norderhaug L, Olafsen T, Michaelsen TE, Sandlie I. Versatile vectors for transient and stable expression of recombinant antibody molecules in mammalian cells. *J Immunol Methods*. 1997; 204:77–87. [PubMed: 9202712]
20. Niesen FH, Berglund H, Vedadi M. The use of differential scanning fluorimetry to detect ligand interactions that promote protein stability. *Nat Protoc*. 2007; 2:2212–2221. [PubMed: 17853878]
21. Varghese R, Mikyas Y, Stewart PL, Ralston R. Postentry neutralization of adenovirus type 5 by an antihexon antibody. *J Virol*. 2004; 78:12320–12332. [PubMed: 15507619]
22. de Martin R, Raidl M, Hofer E, Binder BR. Adenovirus-mediated expression of green fluorescent protein. *Gene Ther*. 1997; 4:493–495. [PubMed: 9274728]
23. Michaelsen TE, Thommesen JE, Ihle O, Gregers TF, Sandin RH, Brekke OH, Sandlie I. A mutant human IgG molecule with only one C1q binding site can activate complement and induce lysis of target cells. *Eur J Immunol*. 2006; 36:129–138. [PubMed: 16323243]
24. Hezareh M, Hessel AJ, Jensen RC, van de Winkel JG, Parren PW. Effector function activities of a panel of mutants of a broadly neutralizing antibody against human immunodeficiency virus type 1. *J Virol*. 2001; 75:12161–12168. [PubMed: 11711607]
25. Baldwin AS Jr. The NF-kappa B and I kappa B proteins: new discoveries and insights. *Annu Rev Immunol*. 1996; 14:649–683. [PubMed: 8717528]
26. Tak PP, Firestein GS. NF-kappaB: a key role in inflammatory diseases. *J Clin Invest*. 2001; 107:7–11. [PubMed: 11134171]
27. Pelegrin M, Naranjo-Gomez M, Piechaczyk M. Antiviral Monoclonal Antibodies: Can They Be More Than Simple Neutralizing Agents? *Trends Microbiol*. 2015; 23:653–665. [PubMed: 26433697]
28. Sapphire EO, Parren PW, Pantophlet R, Zwick MB, Morris GM, Rudd PM, Dwek RA, Stanfield RL, Burton DR, Wilson IA. Crystal structure of a neutralizing human IGG against HIV-1: a template for vaccine design. *Science*. 2001; 293:1155–1159. [PubMed: 11498595]

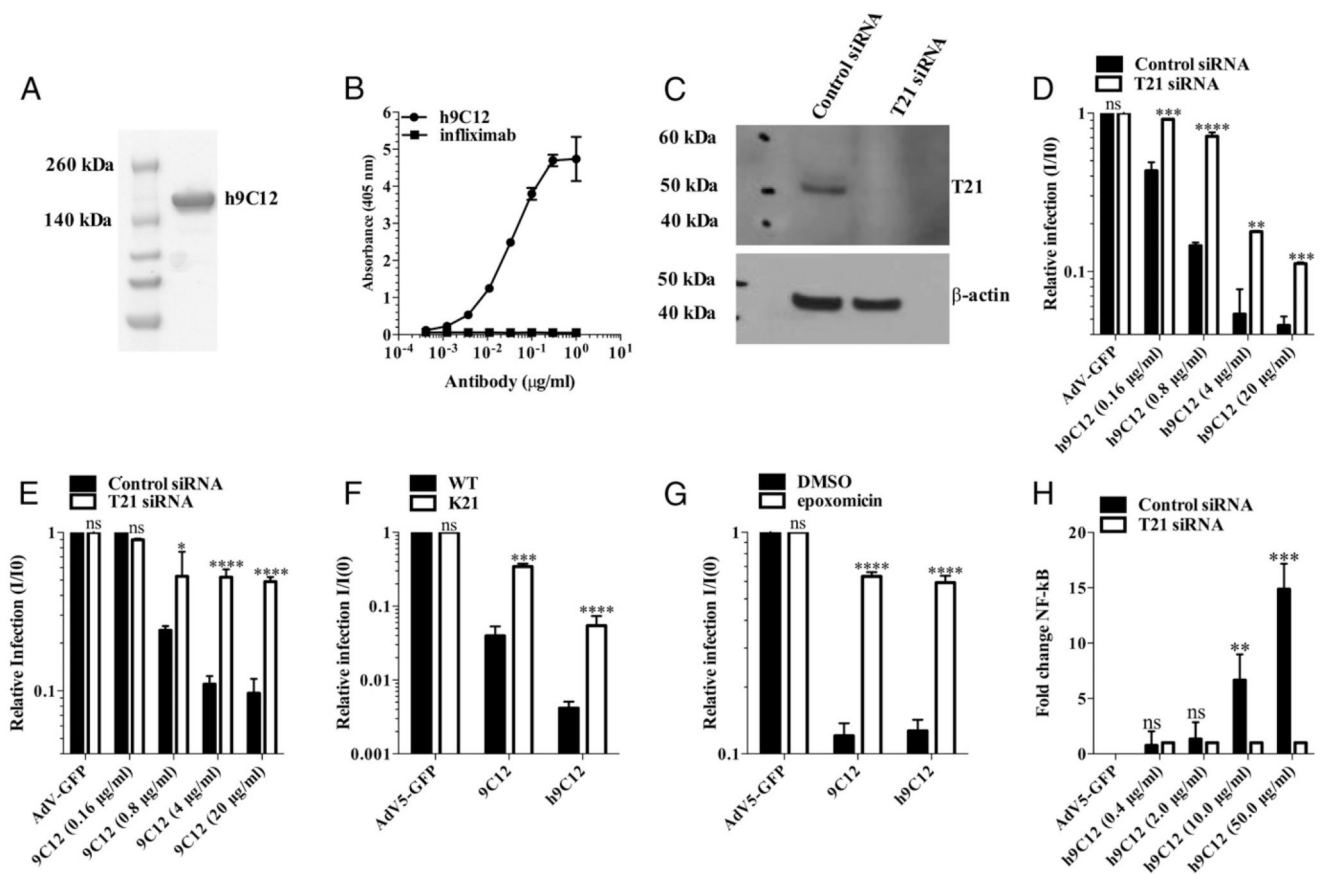


**Figure 1. Construction of a humanized anti-AdV5 IgG1 with antiviral activity.**

(A) Nonreducing SDS-PAGE analysis showing purified monomeric h9C12 produced by HEK293E cells. (B) ELISA showing binding of titrated amounts of h9C12 to its cognate AdV5 hexon Ag. Infliximab (anti-TNF- $\alpha$  IgG1) was used as a negative control. (C) Western blot probed for TRIM21 expression following treatment with control or TRIM21 siRNA.  $\beta$ -actin was used as housekeeping control. (D) Relative infection ( $\log_{10}$ ) of AdV5-GFP in complex with h9C12 in HeLa cells treated with TRIM21 or control siRNA. (E) Relative infection ( $\log_{10}$ ) of AdV5-GFP in complex with the parental murine 9C12 Ab in HeLa cells pretreated with T21 or control siRNA. (F) Relative infection ( $\log_{10}$ ) of AdV5-GFP in complex with 9C12 or h9C12 in WT and K21 MEFs. (G) Relative infection ( $\log_{10}$ ) of AdV5-GFP in complex with 9C12 or h9C12 in HeLa cells treated with DMSO or epoxomicin. (H) Fold change in NF- $\kappa$ B induction in response to infection with AdV5-GFP in complex with WT h9C12 in HEK293T NF- $\kappa$ B reporter cells treated with TRIM21 or control siRNA. Data are presented as fold change from AdV5-GFP only. Error bars represent mean  $\pm$  SD of triplicates from one representative experiment out of three. \* $p$  < 0.05, \*\* $p$  < 0.01, \*\*\* $p$  < 0.005, \*\*\*\* $p$  < 0.001 by multiple unpaired  $t$ -test. ns, not significant.

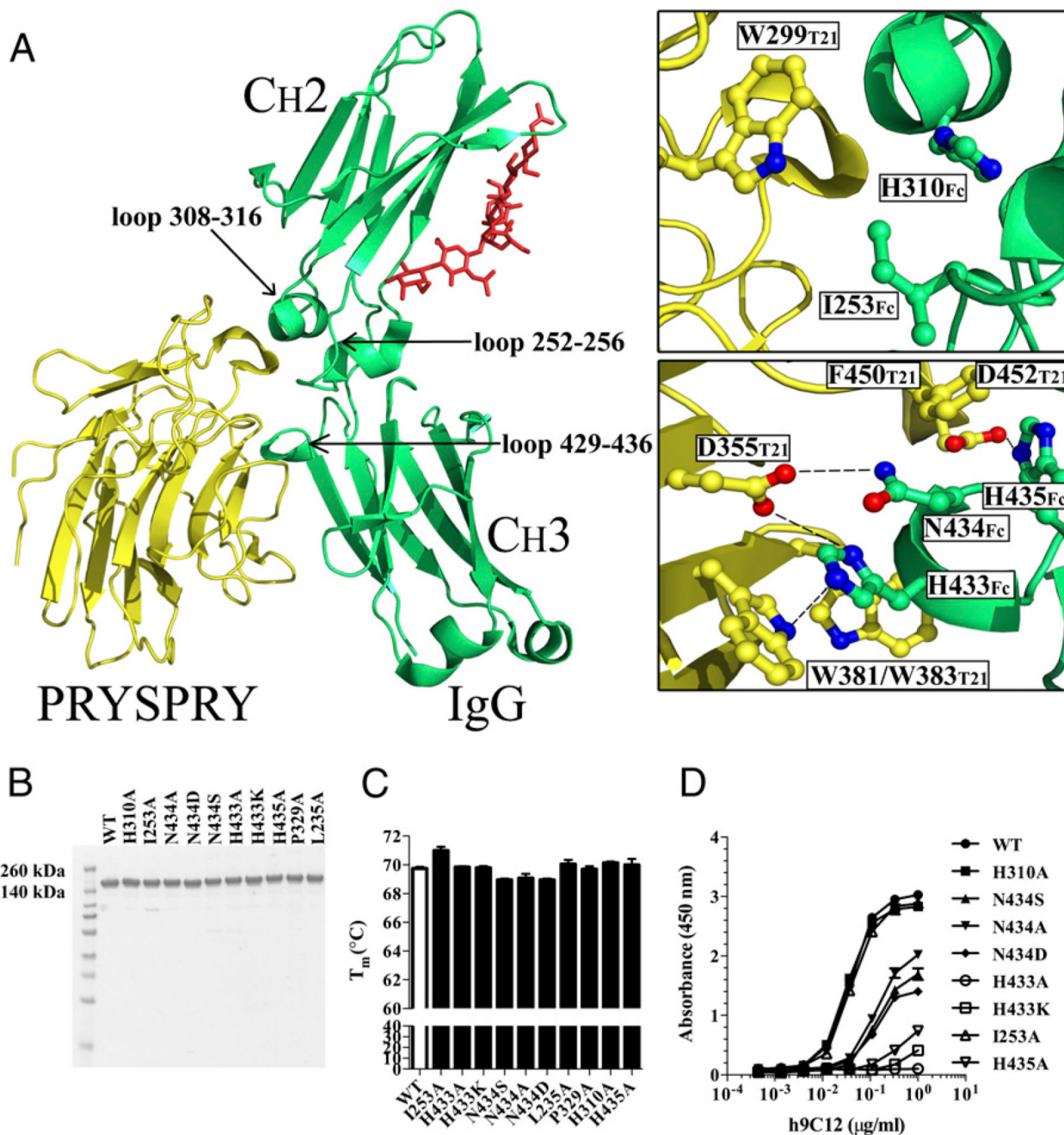


**Figure 2. Production and characterization of Fc-engineered h9C12 variants.**

(A) Illustration of the cocrystal structure of the human TRIM21 PRYSPRY domain (yellow) in complex with a human IgG1 Fc fragment (green). The C<sub>H</sub>2-C<sub>H</sub>3 domains of IgG1 are indicated, and the N-linked glycans attached to N297 of the C<sub>H</sub>2 domains is shown in red. In the C<sub>H</sub>2 domain, the I253<sub>Fc</sub> of loop 252–256 is involved in a hydrophobic interaction with W299<sub>T21</sub>. H310 is shown for reference. In the C<sub>H</sub>3 domain, the H433<sub>Fc</sub> of loop 429–436 interacts via a hydrogen bond with D355<sub>T21</sub> and forms a stable aromatic stacking interaction with W381<sub>T21</sub> and W383<sub>T21</sub>. Furthermore, N434<sub>Fc</sub> interacts via a hydrogen bond with

D355<sub>T21</sub>, whereas H435<sub>Fc</sub> interacts with D452<sub>T21</sub> and is also involved in an aromatic stacking interaction with F450<sub>T21</sub>. The figure was prepared using PyMOL and the Protein Data Bank structure 2IWG (10). **(B)** Nonreducing SDS-PAGE analysis showing fractions of purified monomeric h9C12 variants produced by HEK293E cells. **(C)** A DSF thermal stability bar graph showing the  $T_m$  values for WT h9C12 and Fc-engineered h9C12 variants. **(D)** ELISA showing binding of WT and Fc-engineered h9C12 variants to recombinant MBP-tagged full-length human TRIM21. Error bars represent mean  $\pm$  SD of triplicates from one representative experiment out of three.

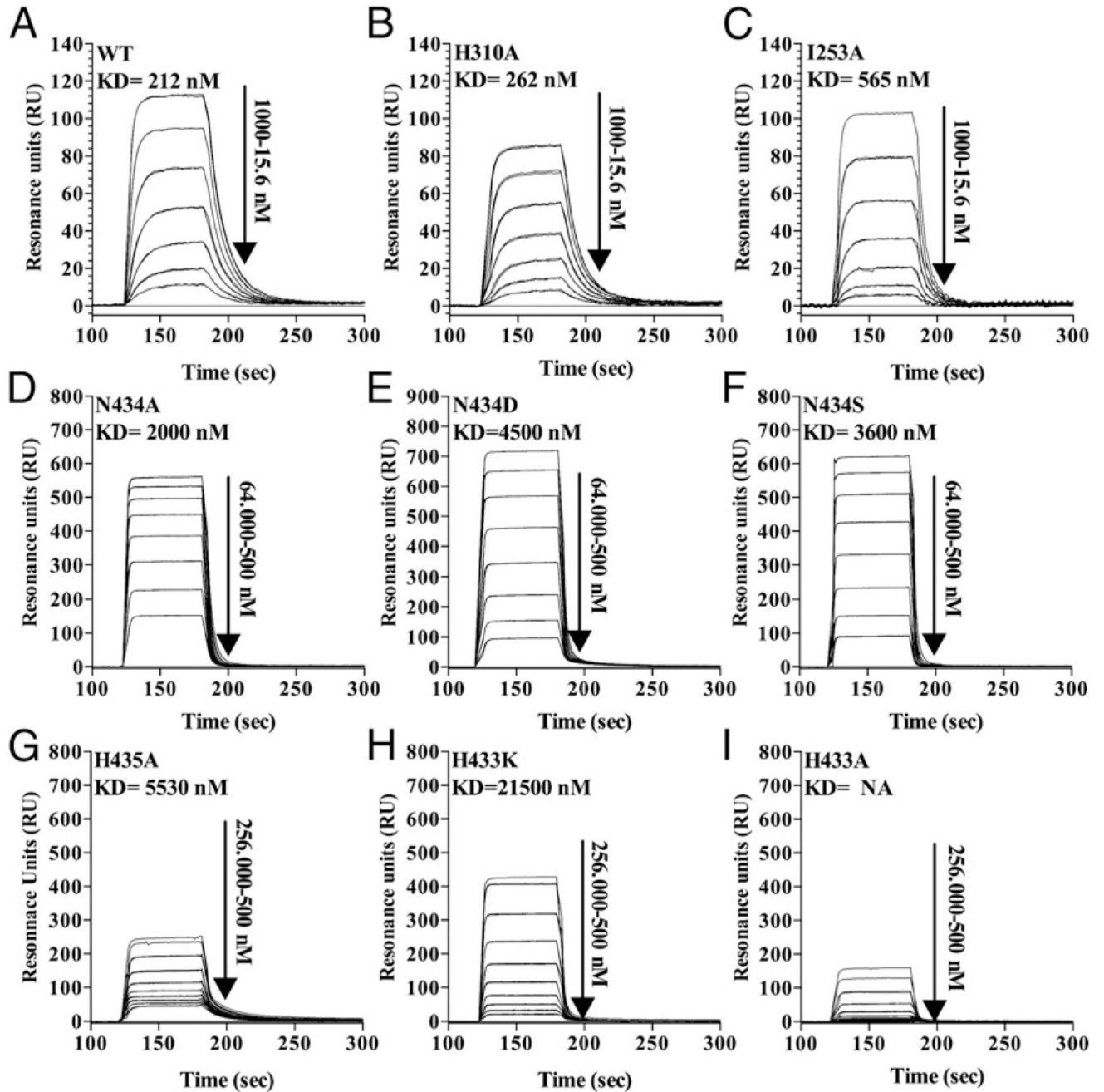


**Figure 3. Altering TRIM21 binding by Fc engineering of h9C12 variants.**

(A–C) Representative sensorgrams showing binding of titrated amounts of recombinant human TRIM21 PRYSPRY (15.6–1000 nM) injected over immobilized h9C12 variants (~550 RU). Representative sensorgrams showing binding of titrated amounts of recombinant human TRIM21 PRYSPRY (500–64,000 nM) (D–F) and (500–256,000 nM) injected over immobilized h9C12 variants (~2500 RU) (G–I). The injections were performed at 25°C, and the flow rate was 40  $\mu$ l/min.

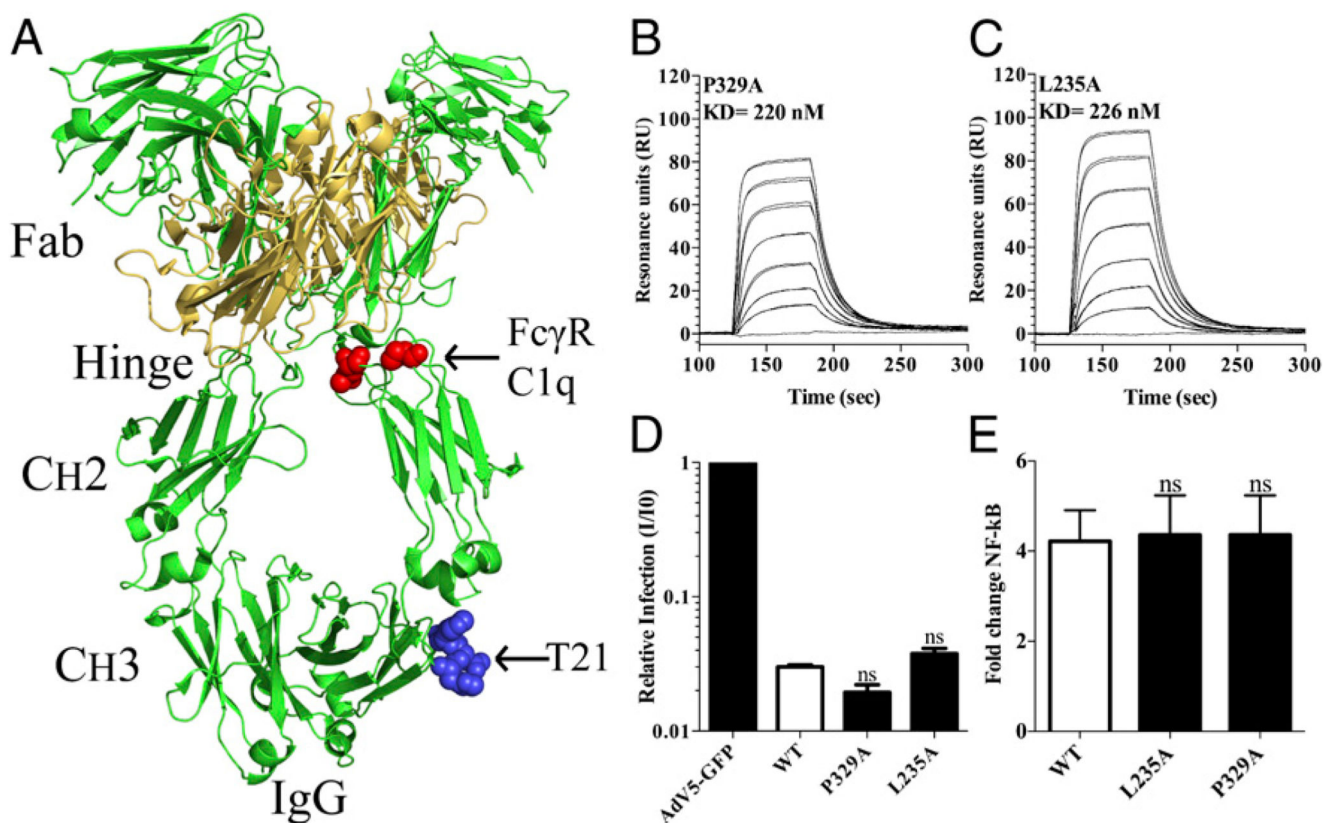


**Figure 4. Neutralization and NF- $\kappa$ B activation by h9C12 variants.**

(A) Illustration showing the crystal structure of full-length human IgG1; key residues required for binding to TRIM21 at the C<sub>H</sub>2-C<sub>H</sub>3 elbow region (H433, N434, and H435; blue), as well as C1q and Fc $\gamma$ R at the upper C<sub>H</sub>2-domain (P329 and L235; red), are highlighted. The human IgG1 H chains are shown in green, and the L chains are shown in yellow. The figure was prepared using PyMOL and the Protein Data Bank structure 1HZH (28). (B and C) Representative sensorgrams showing binding of titrated amounts of recombinant human TRIM21 PRYSPLY (15.6–1000 nM) injected over immobilized h9C12 variants (~550 RU). The injections were performed at 25°C, and the flow rate was 40  $\mu$ l/min. (D) Relative infection (log<sub>10</sub>) of AdV5-GFP in complex with h9C12 variants in HeLa cells treated with DMSO or epoxomicin. Data are presented as fold change versus AdV5-GFP only. (E) Fold change in NF- $\kappa$ B induction in response to AdV5-GFP in complex with h9C12 variants. Data are presented as fold change versus AdV5-GFP only. Error bars represent mean  $\pm$  SD of triplicates from one representative experiment out of three. ns, not significant by one-way ANOVA (Dunnett).

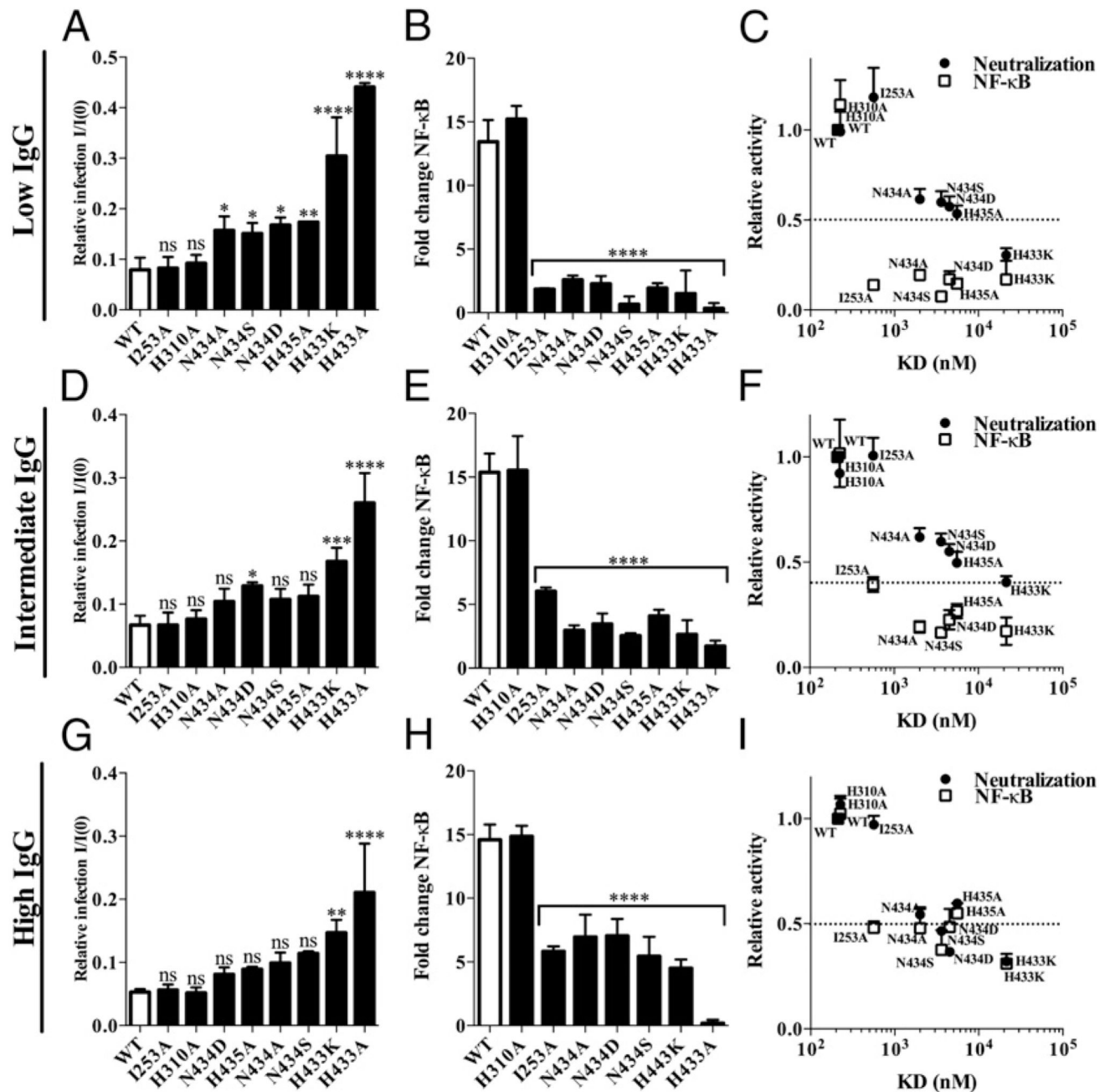


**Figure 5. TRIM21 induction of NF-κB is more sensitive for reduction in IgG affinity than ADIN.** (A) Relative infection of Adv5-GFP in HeLa cells at low level of IgG opsonization. (B) NF-κB induction in response to Adv5-GFP at low level of IgG opsonization. Presented as fold change versus Adv5-GFP only. (C) Dot-plot showing relative ADIN (●) and NF-κB (□) activity as a function of the  $K_D$  values of individual h9C12 variants toward human TRIM21 PRYSPTY at low level of IgG opsonization. (D) Relative infection of Adv5-GFP in HeLa cells at intermediate level of IgG opsonization. (E) NF-κB induction in response to Adv5-GFP at intermediate level of IgG opsonization. Presented as fold change versus Adv5-GFP

only. **(F)** Dot-plot showing relative ADIN (●) and NF-κB (□) activity as a function of the  $K_D$  values of individual h9C12 variants toward human TRIM21 PRYSPRY at intermediate level of IgG opsonization. **(G)** Relative infection of AdV5-GFP in HeLa cells at high level of IgG opsonization. **(H)** NF-κB induction in response to AdV5-GFP at high level of IgG opsonization. Presented as fold change versus AdV5-GFP only. **(I)** Dotplot showing relative ADIN (●) and NF-κB (□) activity as a function of the  $K_D$  values of individual h9C12 variants toward human TRIM21 PRYSPRY at high level of IgG opsonization. Error bars represent mean  $\pm$  SD of triplicates from one representative experiment of three. \* $p < 0.05$ , \*\* $p < 0.001$ , \*\*\* $p < 0.0005$ , \*\*\*\* $p < 0.0001$ , one-way ANOVA test (Dunnett). ns, not significant.

**Table I**

SPR-derived kinetics for binding of h9C12 variants to TRIM21 PRYSPRY

h9C12 Variants	$K_a$ ( $10^4$ /ms)	$K_d$ ( $10^{-2}$ /s)	$K_D$ (nM)
WT	28.2 ± 0.3	6.0 ± 0.2	212.0
P329A	40.5 ± 0.1	6.2 ± 0.1	220.0
L235A	49.6 ± 0.2	6.2 ± 0.1	226.0
I253A	26.3 ± 0.1	17.7 ± 0.2	565.0
H310A	32.5 ± 0.2	8.6 ± 0.1	262.0
H435A	NA	NA	5530.0
N434A	NA	NA	2000.0
N434S	NA	NA	3600.0
N434D	NA	NA	4500.0
H433K	NA	NA	21500.0
H433A	NA	NA	NA

The kinetic rate constants were obtained using a simple first-order (1:1) Langmuir bimolecular interaction model. The kinetic values represent the average of triplicates.

The steady-state  $KD$  values were obtained using an equilibrium (Req) binding model supplied with the BIAevaluation 4.1 software. The affinities derived from equilibrium binding data represent the average of triplicates.

NA, not acquired because of fast binding kinetics.